https://doi.org/10.5194/egusphere-2022-15
Preprint. Discussion started: 23 March 2022

The role of Edge-Driven Convection in the generation of volcanism-part 2: Interactions between Edge-Driven Convection and thermal plumes, application to the Eastern Atlantic

Antonio Manjón-Cabeza Córdoba[1,2] and Maxim D. Ballmer[3,1]

[1]ETH Zürich, Department of Earth Sciences, Institute of Geophysics
[2]University of Oslo, Centre for Earth Evolution and Dynamics
[3]University College London, Deparment of Earth Sciences

Correspondence: Antonio Manjón-Cabeza Córdoba (a.m.c.cordoba@geo.uio.no)

Abstract. In the eastern Atlantic Ocean, several volcanic archipelagos are located close to the margin of the African continent. This configuration has inspired previous studies to suggest an important role of edge-driven convection (EDC) in the generation of intraplate magmatism. In a companion paper (Manjón-Cabeza Córdoba and Ballmer, 2021: The role of Edge-Driven Convection in the generation of intraplate volcanism - part 1: a 2D systematic study, doi:10.5194/se-12-613-2021), we showed that EDC alone is insufficient to sustain magmatism of the magnitude required to match the volume of these islands. However, we also found that EDC readily develops near a step of lithospheric thickness, such as the oceanic-continental transition ("edge") along the western African cratonic margin. In this work, we carry out 3D numerical models of mantle flow and melting to explore the possible interactions between EDC and mantle plumes. We find that the stem of a plume that rises close to a lithospheric edge is significantly deflected ocean-ward (*i.e.*, away from the edge). The pancake of ponding hot material at the base of the lithosphere is also deflected by the EDC convection cell (either away or towards the edge). The amount of magmatism and plume deflection depends on the initial geometric configuration, *i.e.*, the distance of the plume from the edge. Plume buoyancy flux and temperature also control the amount of magmatism, and influence the style and extent of plume-EDC interaction. Finally, comparison of model predictions with observations reveals that the Canary plume may be significantly affected and deflected by EDC, accounting for widespread and coeval volcanic activity. Our work shows that many of the peculiar characteristics of eastern Atlantic volcanism are compatible with mantle-plume theory once the effects of EDC on plume flow are considered.

1 Introduction

Volcanism exerts a major control for material flux between the interior of the Earth and the surface/atmosphere system. Volcanic activity along mid-ocean ridges and subduction zones is readily explained by plate tectonics. However, in the absence of nearby plate boundaries, plate tectonics cannot account for intraplate volcanism.

Several models have been proposed to explain the origin of such magmatism. The leading hypothesis is mantle plume theory, in which a deep columnar thermal anomaly rises from the core-mantle boundary to the base of the lithosphere in order to support

https://doi.org/10.5194/egusphere-2022-15
Preprint. Discussion started: 23 March 2022

localized hotspot volcanism (Wilson, 1963; Morgan, 1971). Still, several predictions of plume theory are not fulfilled at many locations worldwide (*e.g.*, Courtillot et al., 2003) and other models have been put forward: Small Scale Convection (SSC; Richter, 1973; Parsons and McKenzie, 1978; Huang et al., 2003; Dumoulin et al., 2005; Ballmer et al., 2007), Shear-Driven Upwelling (SDU; Conrad et al., 2010) or Edge-Driven Convection (EDC; King and Anderson, 1995, 1998).

In the Eastern Atlantic, several volcanic archipelagos are located on the ocean floor near continental lithosphere. At these locations, many of the predictions of plume theory are not met. For example, in the Canary Islands (where volcanism is as recent as the 2021 eruption of La Palma) volcano ages do not follow a consistent linear age-distance relationship, with coeval volcanism occurring across several hundreds of kilometers (Abdel-Monem et al., 1971, 1972; Thirlwall et al., 2000; Geldmacher et al., 2005), the plume swell is nearly absent (Sleep, 1990; King and Adam, 2014) (although see Huppert et al., 2020), the duration of volcanism at a single island is longer than expected in comparison with other chains (*e.g.* Carracedo, 1999). Besides, a cogenetic relation of these volcanoes with other volcanic fields has been suggested on the basis of geochemistry (Doblas et al., 2007; Duggen et al., 2009). This has led several authors to reject the plume model for these islands (*e.g.* Doblas et al., 2007; Martínez-Arevalo et al., 2013). Similar arguments against the plume model have been made for Cape Verde (King and Ritsema, 2000; Helffrich et al., 2010) or the Cameroon Volcanic Line (Fitton, 1980; Déruelle et al., 2007; Milelli et al., 2012), both of which have also been formed near the African continental margin.

Of the alternative models put forward to substitute mantle-plume theory, EDC is the only one that has been proposed for the three aforementioned volcanic regions (King and Anderson, 1998; King and Ritsema, 2000; Milelli et al., 2012). The EDC model postulates that a convection cell is generated due to the juxtaposition of two lithospheric sections of different age or structure: the related density difference is sufficient to generate a downwelling and an associated upwelling. In theory, the return upwelling flow would be enough to generate magma to sustain ocean island volcanism.

However, in a previous paper (Manjón-Cabeza Córdoba and Ballmer, 2021), we quantitatively tested the hypothesis of Edge-Driven Convection as an origin of oceanic intraplate volcanism near continental margins, and our results showed that, by itself, EDC can only support minor magmatism even under the most favorable conditions, and is clearly insufficient to generate long-lived island-building volcanism. This is consistent with independent studies which found that magmatism is very restricted even at low viscosities and high temperatures (Kim and So, 2020; Duvernay et al., 2021). On the other hand, recent seismic-tomography studies provide evidence for deeply-rooted mantle plumes in the Eastern Atlantic by imaging continuous near-vertical low-velocity anomalies in the mantle (French and Romanowicz, 2015) or broad upwellings just below this archipelagos (Civiero et al., 2021). In addition, additional geophysical evidence points to the presence of thermal upwellings (plumes) at least from the base of the transition zone (Liu and Zhao, 2014; Saki et al., 2015).

In the light of the evidence gathered along these lines, we here explore the dynamics of mantle flow and melting related to plumes that rise near a continental margin (figure 1). We hypothesize that the interaction between plumes and EDC can explain (at least some of) the discrepancies between the predictions of plume theory and observations, as already suggested by Geldmacher et al. (2005). To our knowledge, Plume-EDC interaction has not yet been systematically explored in 3D geodynamic numerical models.

https://doi.org/10.5194/egusphere-2022-15
Preprint. Discussion started: 23 March 2022

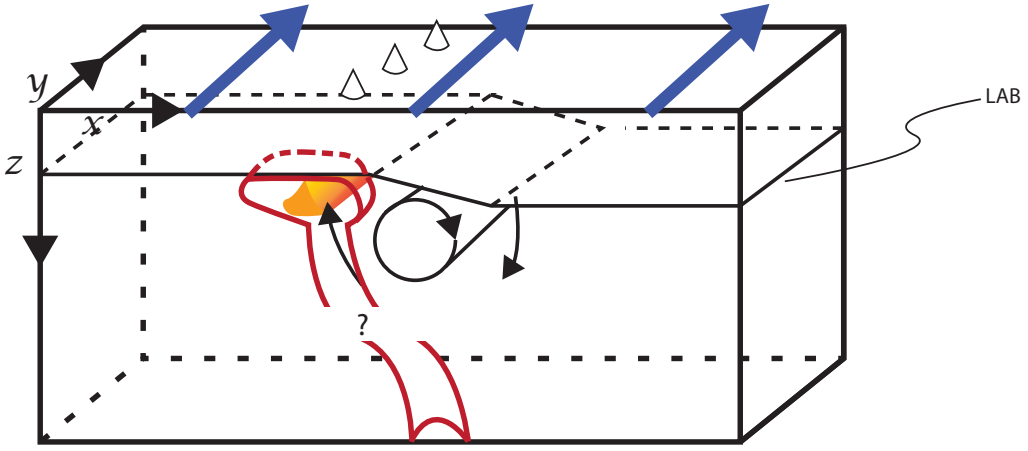

Figure 1. Schematic of a plume interacting with Edge-Driven Convection. In this work, we build on the models of Manjón-Cabeza Córdoba and Ballmer (2021) and add a plume in the form of a temperature anomaly at the bottom, and a plate velocity v_{plate} = 2 cm·yr^{-1} consistent with the age-distance track to the north of the Canary Islands. An idealized Lithosphere-Asthenosphere Boundary (LAB) is labeled in the figure.

To study the interaction between plumes and EDC, we carry out three-dimensional (3D) numerical models of flow and melting near the transition between the oceanic and the continental lithosphere. We explore the parameters that control plume flow (*e.g.*, plume buoyancy flux, plume excess temperature) and EDC (*e.g.*, mantle viscosity, distance of the plume from the continental margin). We conclude that many of the discrepancies between observations and plume theory can be explained by the interaction of deeply-rooted mantle plumes and Edge-Driven Convection, at least for the Canary Islands. We also find that the composition and volumes of magmatism depend on both, plume properties and interaction with sub-lithospheric flow.

2 Methods

We run 3D-Cartesian numerical models using the same version of the finite-element code CITCOM (Moresi and Solomatov, 1995; Moresi and Gurnis, 1996; Zhong et al., 2000) as in our previous paper (Manjón-Cabeza Córdoba and Ballmer, 2021). The conservation equations of mass, momentum and energy are solved on the finite-element mesh; composition is tracked by passive Lagrangian particles (*i.e.*, tracers). 3D geometry of the model box is chosen due to the intrinsic 3D nature of the problem (see figure 1) and the related complex flow patterns. To make our models comparable with the 2D cases in the companion paper (Manjón-Cabeza Córdoba and Ballmer, 2021), we use the same model-box depth z_{box} and width x_{box}. The total extent of our computational domain is 2640×1980×660 km (x_{box}, y_{box}, and z_{box}, respectively). This domain is resolved by a grid of 384×288×96 elements.

https://doi.org/10.5194/egusphere-2022-15
Preprint. Discussion started: 23 March 2022

Kinematic boundary conditions are similar to those in the companion paper. Free-slip is imposed at the side boundaries (x = 2640 km and x = 0 km); no slip is imposed at the bottom. To model Atlantic plate motion and achieve a steady-state for plume inflow and outflow, we impose a plate velocity parallel to the y-direction of v_{plate} = 2 cm·yr^{-1}; and a related Couette flow at the inflow boundary (y = 0 km) that is consistent with the viscosity profile. We acknowledge that the real absolute African plate motion could be oblique to the African margin near the Canaries today, but the volcanic track reflects a history of motion nearly parallel to the African Margin (Geldmacher et al., 2005); in any case, most frames of references depict a plate-movement parallel to the margin (Schellart et al., 2008; Martín et al., 2014). The corresponding outflow boundary (at y = 1980 km) remains unconstrained to allow free exit of material. We also open an unconstrained circular "hole" at the bottom of the box to allow free inflow at the plume location (Ballmer et al., 2011).

The thermal boundary conditions are also similar to those in the previous paper (Manjón-Cabeza Córdoba and Ballmer, 2021). The top boundary is fixed at T_{surf} = 0 °C, while the bottom boundary is fixed at T_{ref} = 1350 °C (+198 °C are added corresponding to the adabatic gradient increase 0.3 K/km × 660 km); the x-normal boundaries are reflective. The models are bottom- and internally heated (H=7.75×10^{-12} W kg^{-1}). At the inflow boundary, the thermal profile corresponds to the initial condition, which is identical to that of the 2D profile of the previous paper (figure 2 in Manjón-Cabeza Córdoba and Ballmer, 2021), including a continental "edge" at x = 1320 km (fig. 2). In nearly all cases of this study, the initial thermal age of the juxtaposed continental and oceanic lithospheres are τ_c = 100 Ma and τ_o = 40 Ma respectively, except for when otherwise specified. This choice of τ_o results in an age of $\tau_{o,y=660}$ = 73 Ma for the oceanic lithosphere right above the plume anomaly.

The width of the (linearly interpolated) transition between the two lithospheric thicknesses is w = 264 km in all cases. In addition, we impose a circular plume thermal anomaly of radius r_{plume} centered at y = 660 km and variable distances from the edge D_{plume} =1320 km - x_{plume}. The plume thermal anomaly is described by:

$$\Delta T = \Delta T_{plume} \cdot e^{\frac{-r^2}{r_{plume}^2}} \quad (1)$$

where ΔT is the difference between the plume temperature and the background temperature, and *r* is the distance from x_{plume}. Plume flux is kept nearly constant during the simulation by automatically adjusting r_{plume} every 50 timesteps. For example, if the plume buoyancy flux $B(t)$ (measured at the bottom boundary) is different from the target value B_{plume} for a given model, r_{plume} is adjusted by a factor of $\frac{B_{plume}}{B(t)}^{0.5}$. This approach keeps $B(t)$ practically constant through much of the simulation, but renders the ratio between the radius of the opening at the bottom of the model and r_{plume} variable between cases. Nonetheless, we make sure that this ratio remains between 3.5 and 4 for all models in the statistical steady state.

The mantle source consists of a mechanical mixture of three different lithological components (depleted/dry peridotite, enriched/hydrous peridotite, pyroxenite), which make up 82 %, 15 %, and 3 % of the volume of the mantle (respectively). We assume that these lithologies are in thermal equilibrium but chemical disequilibrium due to their fine-scale nature (*i.e.*, smaller than the finite-element mesh). Each of these lithologies has a different density and is subject to a different melting law (see companion paper, Manjón-Cabeza Córdoba and Ballmer, 2021; Ballmer et al., 2009). Initially, the lithosphere is depleted in all of the lithologies (see companion paper), and hence is buoyant and does not melt immediately. Progressive melting during

https://doi.org/10.5194/egusphere-2022-15
Preprint. Discussion started: 23 March 2022

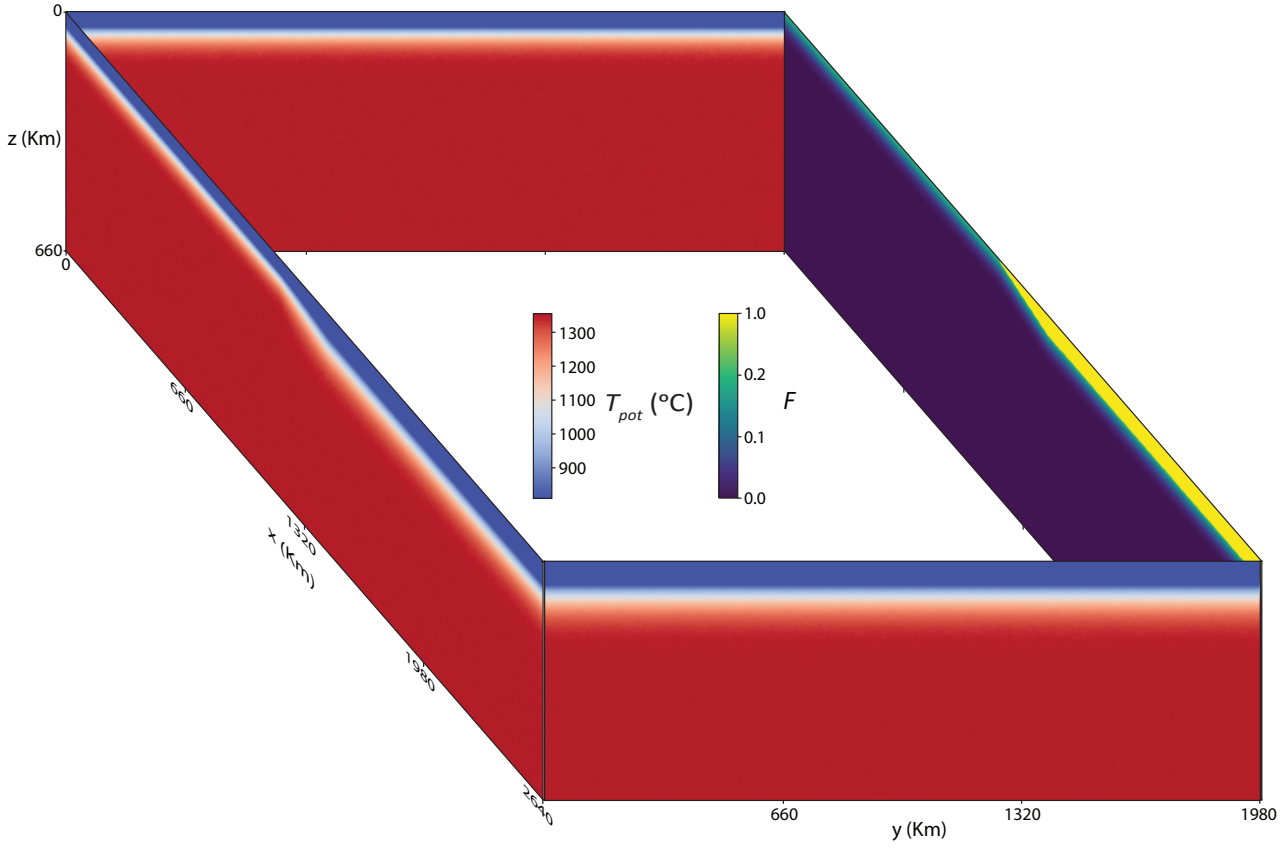

Figure 2. 2D sections depicting the initial thermal (potential temperature) and compositional (depletion for the "depleted component) profiles for the models in this work. Depletion (F) is defined as the amount of melt extracted from the mantle. Plate motion is imposed at the top boundary from left to right. The left side shows the initial thermal and inflow boundary conditions. The right side shows the initial compositional and inflow boundary conditions. The front and back sides show the thermal side boundary conditions. For further details on the calculations of the initial profiles, see Manjón-Cabeza Córdoba and Ballmer (2021).

105 the simulation affects the relevant densities due to melt retention and depletion of the residue. The driving forces (density anomalies) further depend on temperature and composition. In turn, the resisting forces (viscosities) depend on temperature and depth only. For further details, in particular in terms of the density and viscosity ($i.e.$ rheology) parameterizations, we refer the readers to the companion paper (Manjón-Cabeza Córdoba and Ballmer, 2021). Table 1 shows a list of relevant parameters.

https://doi.org/10.5194/egusphere-2022-15
Preprint. Discussion started: 23 March 2022

Table 1. Relevant parameters for the models described in this paper. Values outside and inside of parentheses provide the reference value and the explored parameter space respectively.

Notation	Parameter	Reference value (explored range)	Unit
T_{ref}	Reference temperature	1350	°C
D	Reference thickness	660	km
ρ	Reference density	3300	kg m^{-3}
κ	Thermal diffusivity	1×10^{-6}	m^2 s
g	Gravity acceleration	9.8	m s^2
α	Thermal expansivity	3×10^{-5}	K^{-1}
c_P	Heat capacity (constant pressure)	1250	J kg^{-1} K^{-1}
η_0	Reference viscosity	8.29×10^{18} (5.53×10^{18}-1.24×10^{19})	Pa s
E_a	Activation energy	200	kJ mol^{-1}
V_a	Activation volume	5.00×10^{-6}	m^3 mol^{-1}
γ_a	Adiabatic gradient	0.3	K km^{-1}
H	Internal heating	7.75×10^{-12}	W kg^{-1}
F	Melt depletion	0-1	-
v_{plate}	Plate velocity	2	cm yr^{-1}
B_{plume}	Buoyancy flux	100 (50-500)	kg s^{-1}
ΔT_{plume}	Excess temperature of the plume	150 (100-200)	°C
D_{plume}	Distance of the plume thermal anomaly from the edge	0 (0-400)	km

3 Results

In the 2D models of the companion paper (Manjón-Cabeza Córdoba and Ballmer, 2021), we find that EDC starts right at the onset of the model evolution with a dominant downwelling below the continental side of the edge (or ocean-continent transition), and a return-flow upwelling below the oceanic side. The upwelling sustains erosion of the lithosphere, creating a "bump" or "dent" at its base. Ultimately, SSC also occurs at the base of the oceanic lithosphere far from the edge. We refer to SSC as thermal-boundary layer instability that (in contrast to EDC)) is not immediately triggered by the presence of a nearby edge, but rather typically occurs as soon as the boundary layer (nearly) reaches its critical thickness (Richter, 1973; Parsons and McKenzie, 1978).

In this study, test cases without a mantle plume confirm that the results of Manjón-Cabeza Córdoba and Ballmer (2021) are robust and hold in our 3D geometry: EDC begins right after the material enters the model box, promoting a convection cell and related sub-lithospheric erosion above the upwelling on the oceanic side. SSC develops in our 3D models, appearing sooner

https://doi.org/10.5194/egusphere-2022-15
Preprint. Discussion started: 23 March 2022

(*i.e.*, closer to the inflow boundary) near the edge than far away for it, with convection cells typically aligned parallel to plate motion as "Richter rolls" (Richter, 1973; Richter and Parsons, 1975; Marquart, 2001; Huang et al., 2003). The development of Richter Rolls is stable even for our low v_{plate} = 2 cm/yr (Korenaga and Jordan, 2003, *cf.*[).

Figure 3 shows the results of the reference case, which includes a plume with ΔT_{plume} = 150 °C, B_{plume} = 100 kg·s^{-1}, and D_{plume} = 0 km. Compared to other geodynamic studies of mantle plumes (Ribe and Christensen, 1994; Ballmer et al., 2011), the most evident characteristic of this model is the lateral deflection of the plume conduit. Instead of ascending vertically, the plume conduit is displaced towards the oceanic side with thinner lithosphere. This displacement suggests some interaction of plume flow with EDC-related flow.

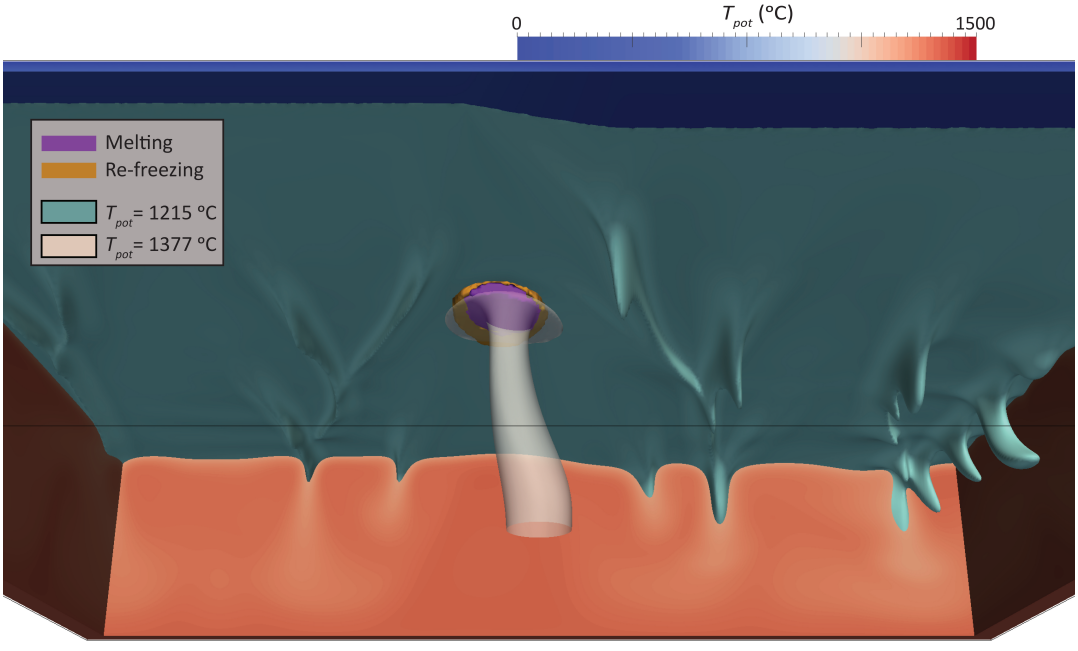

Figure 3. Steady-state temperature field and melting for the reference case with ΔT_{plume} = 150 °C, B_{plume} = 100 kg·s^{-1}, D_{plume} = 0 km, and η_0 = 8.29·10^{18} Pa·s. Cross sections of potential temperature (at the margins of the model) are shown in red-to-blue colors. The light blue and white surfaces mark isotherms (as labeled), showing the base of the lithosphere and the plume, respectively. The purple contour outlines the region of active melting while the orange contour outlines the region of finite melt presence, including where active melt re-freezing occurs.

The plume ponds at the base of the lithosphere as a pancake of hot material. The hottest central part of the plume pancake is located at the minimum thickness of the oceanic lithosphere (*i.e.* at the aforementioned "dent" or "bump"). Without further analysis, however, it remains unclear whether the plume is conveyed to this minimum thickness created by EDC, or if the plume actively creates a dent, and EDC reorganizes accordingly. The plume pancake and melting zones are slightly asymmetric, but

https://doi.org/10.5194/egusphere-2022-15
Preprint. Discussion started: 23 March 2022

again: it remains unclear whether this asymmetry is due to the spreading of the pancake at the base of a lithosphere with variable thickness at the ocean-continent transition, or it is caused by EDC-related flow.

In the reference case, the plume acts to efficiently erode the imposed edge at the base of the lithosphere, displacing the thermal boundary layer and the main EDC downwelling continent-wards. This erosion also creates a Plume Erosion Track (PET) that is observed in all models Ribe and Christensen (1994). In the reference case (fig. 3), the PET is mostly parallel to the direction of plate motion.

To better quantify the lateral displacement of the plume stem and the pancake, we calculate a Plume Deflection Index (PDI) defined simply as the inverse of the slope ($\frac{\Delta x}{\Delta z}$) between two temperature maxima at two different depths. PDI_{stem} is a proxy for the plume-stem displacement, calculated as the lateral distance between the plume stem (and related thermal maxima) at z = 220 km and at z = 660 km (divided by the difference between both these depths, *i.e*, 440 km); in addition, we also report a $\text{PDI}_{pancake}$, which is calculated from the thermal maxima at depths of z = 110 km and z = 220 km, and otherwise analogously to PDI_{stem}. In this work, we arbitrarily define positive values of PDI as distortions of upwelling flow "away from the edge" and negative values as "towards the edge". In the reference case, PDI_{stem} = 0.143 and $\text{PDI}_{pancake}$ = 0.109. Both the stem and the pancake are deflected towards the oceanic side. These values correspond to absolute displacements of the plume towards the oceanic domain of 63 km from 660 km to 220 km depth, an another 12 km from 220 km to 110 km depth. In particular, the lateral displacement of the plume stem is significant. We will discuss the relevance of these values in comparison to other cases below.

We also investigate the compositional origin of mantle melts as a proxy for their geochemical signature. To do this, we evaluate the total melt volume flux M (*i.e.*, melt produced in the mantle) and total volcanic volume flux V (*i.e.*, melt extracted from the mantle), along with the melt flux and volcanic flux that is related to pyroxenite melting only: M_{PX} and V_{PX}, respectively. These metrics provide a compositional index for mantle melting, $\frac{M_{PX}}{M}$, and melt extraction, $\frac{V_{PX}}{V}$. The latter is the compositional origin of volcanism explicitly predicted by our models. Note, however, that this specific predicition of lithological origins depends on the critical porosity explicitly assumed here (1 %), and on the style of melt extraction. For example, if pyroxenite-derived and peridotite-derived melts were already pooled in the mantle (instead of in a shallow magma chamber), and then were extracted together, or if all melts were efficiently extracted (*i.e.*, for fully fractional melting), $\frac{M_{PX}}{M}$ would provide a more appropriate geochemical proxy than $\frac{V_{PX}}{V}$. In other words, both $\frac{M_{PX}}{M}$ and $\frac{V_{PX}}{V}$ provide reasonable bounds for the compositional origin of predicted lavas.

In the reference case, $\frac{M_{PX}}{M}$ and $\frac{V_{PX}}{V}$ are 0.774 and 0.994, respectively. Such a dominance of pyroxenite-derived melting and volcanism is mostly explained by the relatively low plume excess temperatures and large relative seafloor ages modeled here (and relevant for Eastern Atlantic Volcanism; Müller et al., 2008). The related large lithospheric thicknesses restricts extensive peridotite melting, even though peridotite is the most abundant component in the plume source. Also note that pyroxenite melting starts at greater depths than peridotite melting and efficiently extracts latent heat, such that the ascent of peridotitic material is sub-adiabatic (less melting) and the ascent of pyroxenite material is super-adiabatic (more melting, Hirschmann and Stolper, 1996).

https://doi.org/10.5194/egusphere-2022-15
Preprint. Discussion started: 23 March 2022

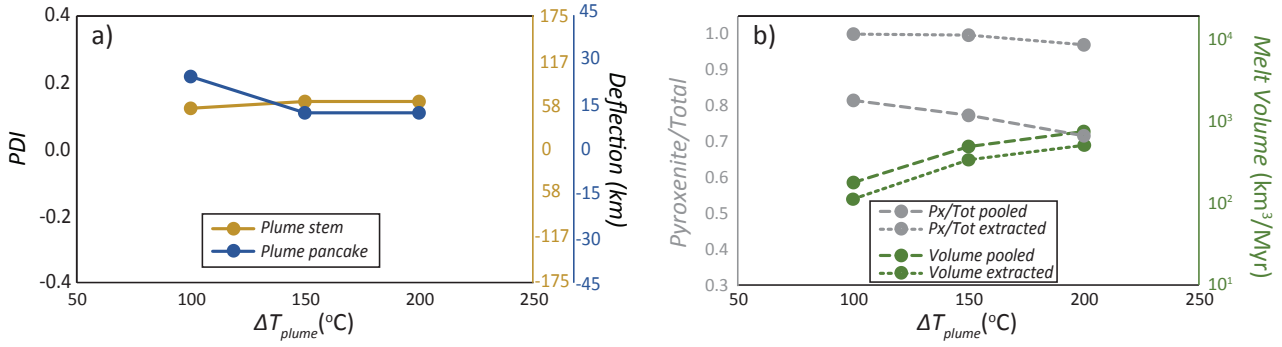

Figure 4. Diagrams showing the sensitivity of several output parameters as a function of ΔT_{plume}. (a) Plume Distortion Index (PDI) for the different models (see text for explanation). Note that all values are positive (deflection away from the edge). (b) Melt volumes fluxes (M and V) and melt compositional index ($\frac{M_{PX}}{M}$ and $\frac{V_{PX}}{V}$) for the different models. Predictions in terms of melt production (M, $\frac{M_{PX}}{M}$) are given as dashed lines; predictions in terms of melt extraction (V, $\frac{V_{PX}}{V}$) as dotted lines.

3.1 Effects of plume temperature

We conduct a series of cases with variable plume excess temperature ΔT_{plume} and constant buoyancy flux B_{plume}. We find that ΔT_{plume} has only minor effects on the overall flow patterns at a given B_{plume}. As B_{plume} is kept constant, the radius of a hotter plume is implicitly smaller than that of a cooler plume. As a consequence of this implicit effect of ΔT_{plume} on plume radii, the plume pancake and the related PET tend to be wider for smaller ΔT_{plume}. Nonetheless, the base of the lithosphere is eroded more efficiently for large ΔT_{plume}, because a hotter plume sustains a lower-viscosity pancake, which more efficiently destabilizes the very base of the lithosphere.

There is no indication that changing ΔT_{plume} while keeping B_{plume} constant systematically changes the effect of EDC-related flow on plume ascent. The lateral displacement of the plume by EDC is similar across all our models with different ΔT_{plume}, as evidenced by the nearly flat trends of PDI_{stem} and $\text{PDI}_{pancake}$ lines (figure 4a). The only noticeable difference between the models is that the plume pancake is more asymmetric for the case with ΔT_{plume} = 100 °C than for greater ΔT_{plume}. Note also that all PDIs in Figure 4a are positive, implying that the plume is consistently deflected away from the edge at all depths.

Melt fluxes (*i.e.*, volume fluxes of melts produced in the mantle) and volcanic fluxes (*i.e.*, volume fluxes of melts extracted from the mantle) systematically increase with ΔT_{plume} (fig. 4b). This result is intuitive, and consistent with previous work (Ribe and Christensen, 1994; Ballmer et al., 2011). In terms of the compositional origin of magmas, $\frac{M_{PX}}{M}$ and $\frac{V_{PX}}{V}$ decreases with the amount of melt produced, and therefore decreases with increasing ΔT_{plume} (fig. 4b). This result is expected as PX-derived melts are diluted by peridotite-derived melts for increasing degrees of melting.

https://doi.org/10.5194/egusphere-2022-15
Preprint. Discussion started: 23 March 2022

3.2 Effects of Plume Buoyancy Flux

We also explore the influence of B_{plume} on model results. Figure 5 shows steady-state model predictions for cases with different B_{plume}, but otherwise the same parameters as in the reference case. Increasing B_{plume} implicitly increases the radius of the plume. Thereby, the width and volume of the melting zone and of the plume pancake also increase, as does the area of PET. The PET remains mostly parallel to plate velocities, as for the reference case.

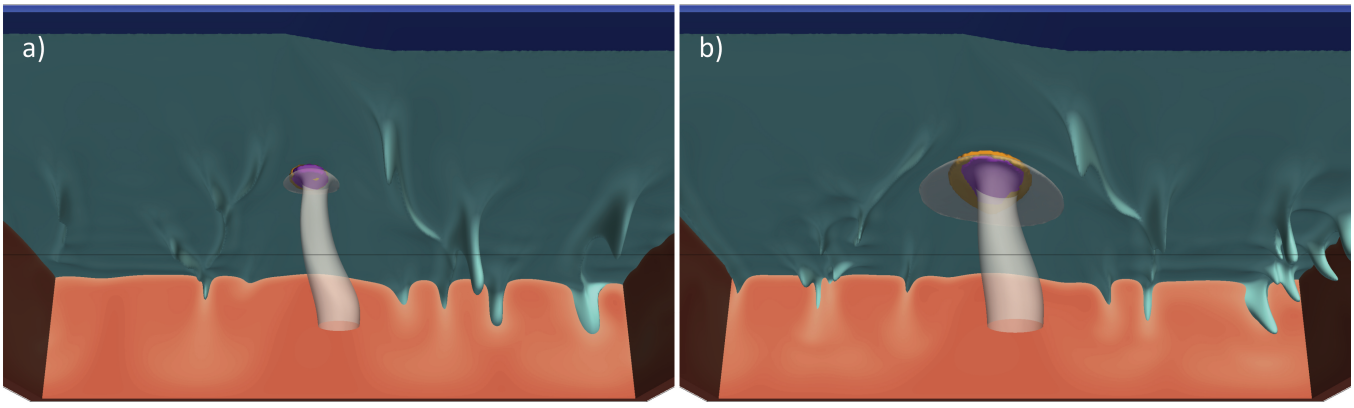

Figure 5. Steady-state snapshots of representative cases with different B_{plume} but otherwise the same parameters as in the reference case (Figure 3). (a) B_{plume} = 50 kg·s^{-1}; (b) B_{plume} = 200 kg·s^{-1}. For reference to colors of surfaces and cross-sections, see figure 3 caption and legend.

The lateral deflection of the plume stem is less evident for cases with higher than for cases with lowerB_{plume}. Indeed, the high buoyancy-flux plume rises more straightly through the model box than the plume in the reference case. In fact, PDI$_{stem}$ tends to 0 as B_{plume} increases (Fig. 6a,c), providing evidence for a limitation of the ability of EDC (or of SSC in general) to affect the rise of plumes: efficient displacement is restricted to plumes with moderate-to-low buoyancy fluxes. Nevertheless, the melting zone and the plume pancake display subtle asymmetry also in the case with the highest B_{plume} modeled here. As for PDI$_{stem}$, PDI$_{pancake}$ also tends to decrease for increasing B_{plume}, but remains positive.

Due to the aforementioned radius increase as a function of B_{plume}, M and V both systematically increase with increasing B_{plume}. Regarding melt compositions, $\frac{M_{PX}}{M}$ and $\frac{V_{PX}}{V}$ display a shape that mirror melt volumes (Figure 6b,d), decreasing with increasing B_{plume}. Similar to the effects of plume excess temperature (see figure 4), the trends of melt volumes and compositions as a function of B_{plume} mirror each other, because $\frac{M_{PX}}{M}$ and $\frac{V_{PX}}{V}$ decrease with increasing degrees of melting of the dominant lithology, peridotite.The influence of B_{plume} on magma compositions decreases at higher buoyancy fluxes, probably because the extent of vertical sublithospheric erosion becomes nearly independent of B_{plume} at some point. Note that the convex upward shape of the dotted grey line in fig. 6 is due to the saturation of PX contributions at ∼100%. In figure 6, the difference in composition between the produced melts and the extracted melts is greater for lower ΔT_{plume}, which is not evident in figure 4. This is explained by the much higher productivity of pyroxenite melting (and hence: smaller sensitivity to

https://doi.org/10.5194/egusphere-2022-15
Preprint. Discussion started: 23 March 2022

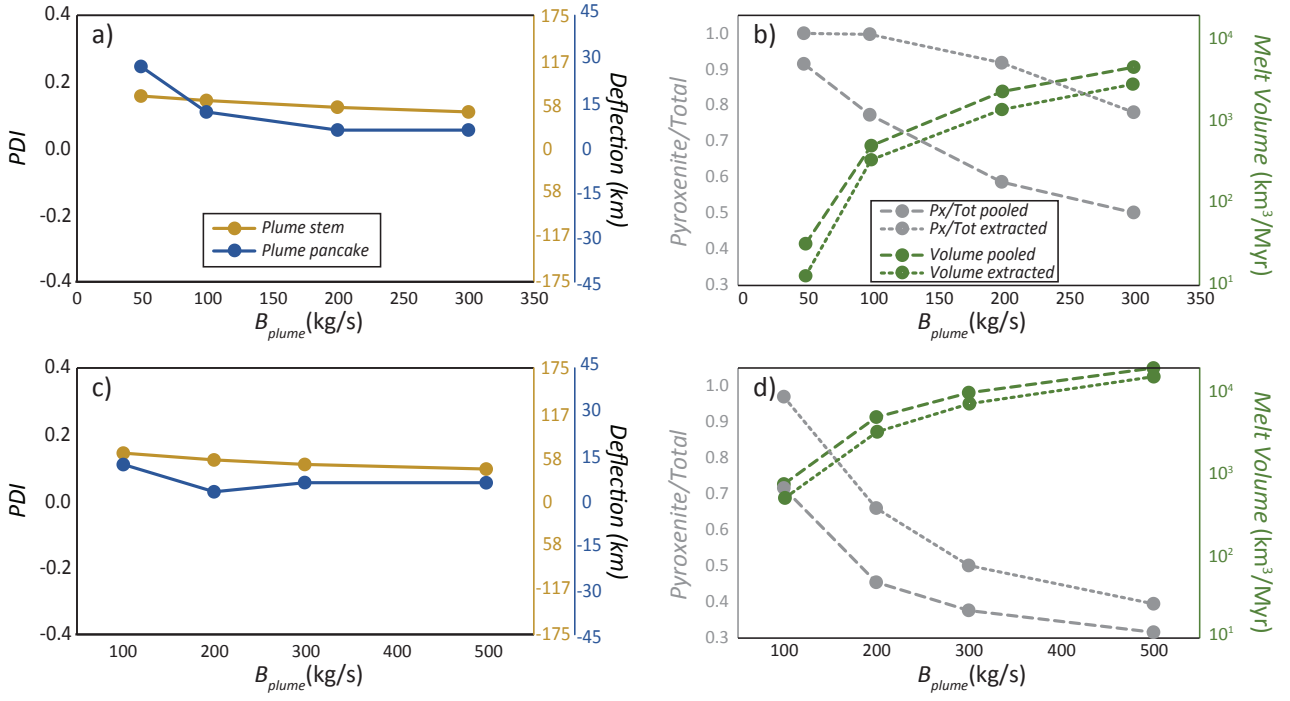

Figure 6. Diagrams showing the variation of key output parameters to changing B_{plume}. (a) PDI_{stem} and $\text{PDI}_{pancake}$ for models with variable B_{plume} and ΔT_{plume} = 150 °C. (b) M, V, $\frac{M_{PX}}{M}$, and $\frac{V_{PX}}{V}$ for models with variable B_{plume} and ΔT_{plume} = 150 °C. (c) Same as (a) for models with ΔT_{plume} = 200 °C. (d) Same as (b) for models with ΔT_{plume} = 200 °C.

an extraction threshold) than for peridotite melting at high B_{plume}. Among all the parameters explored in this work, B_{plume} shows the strongest effect on plume vigor and related melting.

3.3 Effects of distance of the Plume from the Edge

Next, we analyze the effects of the distance of the base of the plume from the edge, D_{plume}, on model results as well. The effects of this parameter are a good indicator of plume-EDC interaction, because D_{plume} changes the spatial relationship between the plume and the edge, while leaving intrinsic plume parameters unchanged. Figure 7 shows 3D snapshots of mantle temperature and melting as a function of D_{plume} for two sets of ΔT_{plume} and B_{plume} (in the top row, for a relatively weak plume with parameters such as in the reference case: ΔT_{plume} = 150 K and B_{plume} = 100 kg·s^{-1}; and the bottom row, for a moderately strong plume with ΔT_{plume} = 200 K and B_{plume} = 200 kg·s^{-1}). Interaction of the plume with the EDC convection cell and topography at the base of the lithosphere causes systematic changes in the flow patterns and related melting characteristics. For D_{plume} = 200 km (fig 7a,c) the plume stem is deflected in a similar way as in the reference case (figure 3), for which D_{plume} = 0 km. For D_{plume} = 400 km, the plume stem is instead generally less affected by the presence of the edge and related EDC.

https://doi.org/10.5194/egusphere-2022-15
Preprint. Discussion started: 23 March 2022

Regarding the plume pancake, we find two significant changes in the behavior predicted by our cases with variable D_{plume} with respect to the reference case (figure 3). First, as the plume is shifted away from the edge (*i.e.*, for increasing D_{plume}), the plume pancake is deflected towards the edge. This transition happens at a different D_{plume} depending on plume properties (∼25 km in figure 8a, ∼125 km in 8c), but it happens nonetheless. After this rather sudden transition, the edge-ward deflection of the pancake decreases progressively with increasing D_{plume}. At a distance of D_{plume}= 400 km, another notable phenomenon occurs: vigorous SSC occurs in the plume pancake with dominant transverse rolls (*i.e.*, perpendicular to the edge). This peculiar geometry of SSC separates the plume-fed melting zone into two distinct melting zones (figure 7b,d). This separation is transient, however: as the SSC downwellings move with the plate, the two melting zones are separated and merged periodically. The fact that transverse SSC rolls in the plume pancake only occur at D_{plume} = 400 km suggests that this phenomenon is either a consequence of the interaction of EDC and plumes at a particular D_{plume}, or hindered by EDC at any other D_{plume}. In any case, a similar geometry of SSC has been found in studies of plumes without a nearby edge (Ballmer et al., 2011), or studies of EDC without a plume present (Kaislaniemi and Van Hunen, 2014).

Figure 8 shows the effect of D_{plume} on quantitative characteristics of plume ascent. Note that the significant changes shown in figure 8, both in terms of PDI and melt fluxes as a function of D_{plume}, are exclusively due to plume-EDC interaction (intrinsic plume parameters remain unchanged in each row of figure 8). PDI_{stem} is generally positive, but highly variable. It peaks at D_{plume} = 50 km and D_{plume} = 150 km for the relatively weak and strong plumes shown in the top and bottom rows of figure 8, respectively. For higher D_{plume}, PDI_{stem} systematically decreases with D_{plume}. In turn, $\text{PDI}_{pancake}$ becomes strongly negative for the D_{plume} at which PDI_{stem} peak, and progressively less negative for any higher D_{plume}. These results emphasize the strong effects of plume-EDC interaction, and its diversity as a function of D_{plume} (and for plumes with different ΔT_{plume} and/or B_{plume}). The switch to dominantly transverse rolls in the pancake for plumes far from the edge (*i.e.* at D_{plume} = 400 km) does not seem to strongly affect the deflection of the plume stem or shallow pancake.

Compared to PDI, the effects of D_{plume} on melt fluxes and compositions are less severe. Figure 8b,d show the trends of melting-related parameters as a function of D_{plume} at the same scale than other figures (*e.g.*, figure 6). The effects on melt fluxes appear small, which is mostly due to the logarithmic scale of the figure; nonetheless several 'regimes' or different behaviors can be distinguished on the basis of distance of the plume to the edge. Similar to the PDI figure, there is an initial regime (D_{plume} = 0 km for the cases with B_{plume} = 100 kg·s^{-1}; and D_{plume} = 0-100 km for the cases with B_{plume} = 200 kg·s^{-1}) with lower PDI, and the melting volumes remain mainly flat (at least in figure 8d). Then, at greater distances, EDC interacts strongly with the plume, resulting in slightly lower melting volumes with a smooth peak around D_{plume} = 200 km. Finally, at D_{plume} = 400 km, melting volumes increase substantially due to SSC, but volcanism remains practically the same (suggesting that the main volume of melting still happens at the top of the plume conduit).

In general, plume deflection, as caused by the effects of EDC, tends to systematically decrease the amounts of hotspot magmatism for a given plume vigor/temperature. The least negative (or most constructive) plume-EDC interaction occurs near D_{plume}=0 km and D_{plume}=200 km. These locations roughly reflect the intrinsic pattern of the EDC-related and neighboring "triggered" SSC-related upwellings, as predicted by the companion paper, but not exactly so. The differences being likely due to the effect of the presence of a plume on EDC and SSC patterns. That the distance of the change of regime (from little

https://doi.org/10.5194/egusphere-2022-15
Preprint. Discussion started: 23 March 2022

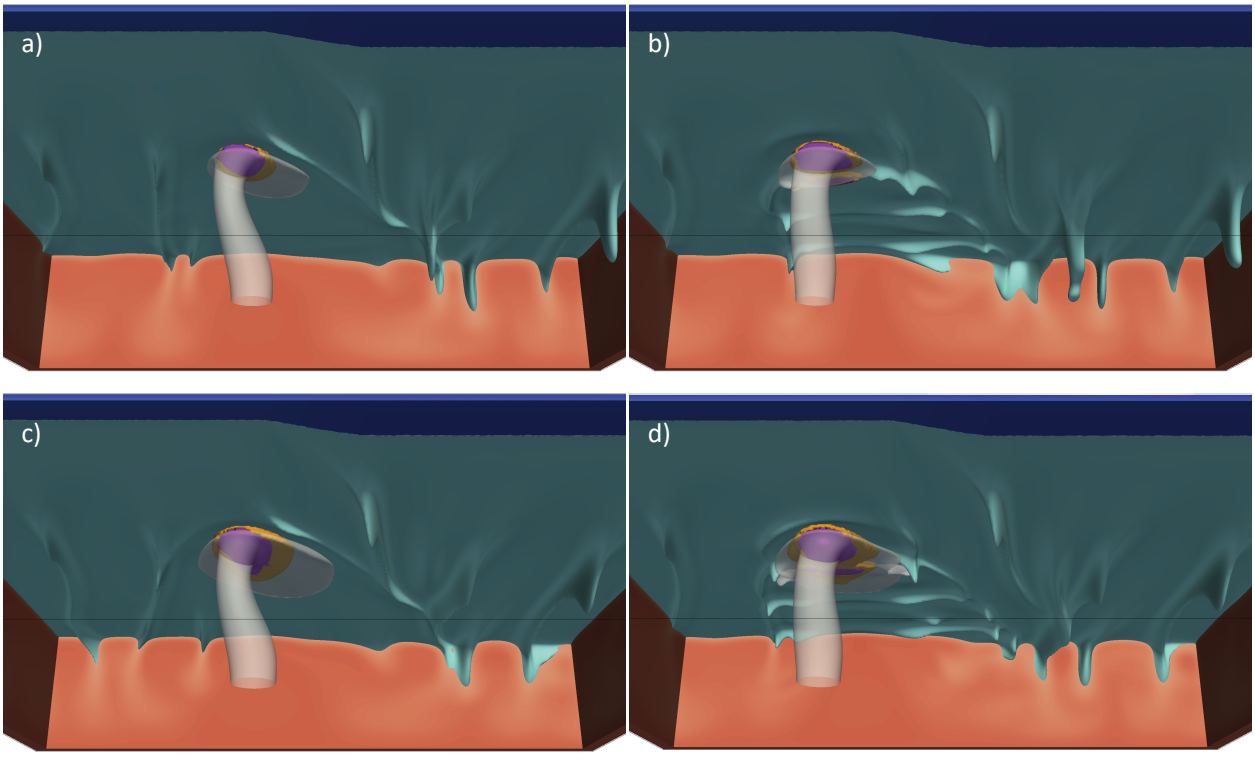

Figure 7. Steady-state snapshots of representative cases with variable D_{plume}. (a,c) Cases with D_{plume} = 200 km. (b,d) Cases with D_{plume} = 400 km. In the top row, models with a relatively weak plume with ΔT_{plume} = 150 °C and B_{plume} = 100 kg·s^{-1} are shown. In the bottom row, models with a relatively strong plume with ΔT_{plume} = 200 °C and B_{plume} = 200 kg·s^{-1} are shown. For reference to colors of surfaces and cross-sections, see fig. 3 caption and legend.

to strong) of influence of EDC on the plume depends on plume vigor is also related to the effects of the plume (and plume pancake) on the wavelength of EDC. Thus, EDC appears to affect plume ascent and vice-versa.

Similar to our findings for PDI$_{pancake}$, the PET is deflected towards the continental side as an effect of EDC flow downstream from the hotspot. The PET is also affected by the SSC in the plume pancake perpendicular to plate motion. Very likely, these predictions have implications for dynamic topography and swell geometry. Very likely, these predictions have implications for dynamic topography and swell geometry.

3.4 Effects of mantle viscosity

Finally, we explore models with different reference viscosities. Figure 9 shows data for cases with variable viscosity, D_{plume} = 200 km, and otherwise the same parameters as in the reference case. Similar to the effects of plume temperature, the width of

https://doi.org/10.5194/egusphere-2022-15
Preprint. Discussion started: 23 March 2022

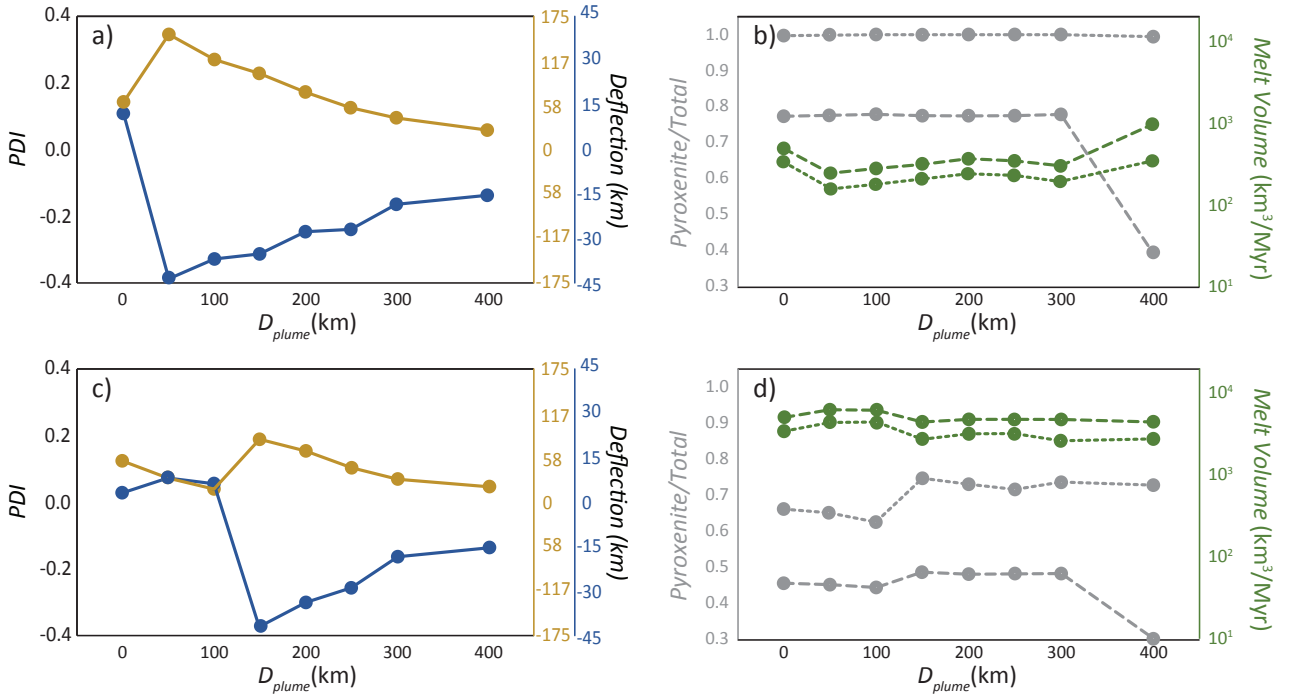

Figure 8. Diagrams showing the sensitivity of key output parameters to D_{plume}. (a,c) PDI_{stem} (light brown) and $PDI_{pancake}$ (blue) in the steady state for models with variable D_{plume}. (b,d) M, V, $\frac{M_{PX}}{M}$, and $\frac{V_{PX}}{V}$, for models with variable D_{plume}. In the top row, results for a relatively weak plume with ΔT_{plume} = 150 °C and B_{plume} = 100 kg·s^{-1} are given. In the bottom row, results for with a relatively strong plume with ΔT_{plume} = 200 °C and B_{plume} = 200 kg·s^{-1} are given. Legend as in figures 4, 6.

the plume stem is implicitly smaller with decreasing reference viscosity. One of the most striking characteristics of these cases is that the deflection of the plume stem is less severe for the high-viscosity and the low-viscosity case than for the intermediate-viscosity case, shown in figure 7c (same distance and same B_{plume}, but intermediate η_0). Indeed, PDI indexes (fig. 9a) display a maximum in terms of plume deflection for the intermediate viscosity value of the reference case η_0 = 8.29·10^{18} Pa·s (figure 3).

Since the vigor of EDC decreases with increasing η_0 (Manjón-Cabeza Córdoba and Ballmer, 2021), and thus EDC-plume interaction should also become less important, this result is not obviously intuitive. That an expected systematic trend of decreasing PDI with increasing η_0 is not fully supported by the cases in figure 9 may indicate that the D_{plume} at which the strongest plume-EDC interaction occurs depends on η_0 (the previous sub-section demonstrates that it also depends on ΔT_{plume} and B_{plume}). Indeed, the preferred wavelength of EDC/SSC also depends on η_0.

In turn, model predictions in terms of melting as a function of η_0 are as expected. Both M and V increase with decreasing η_0 and, along with this decrease, $\frac{M_{PX}}{M}$ and $\frac{V_{PX}}{V}$ decrease (figure 9b). In addition to plume-related hotspot melting, melting away from the hotspot (*i.e.* directly due to EDC) appears for the case with low η_0 . This melting is minor and consistent with

https://doi.org/10.5194/egusphere-2022-15
Preprint. Discussion started: 23 March 2022

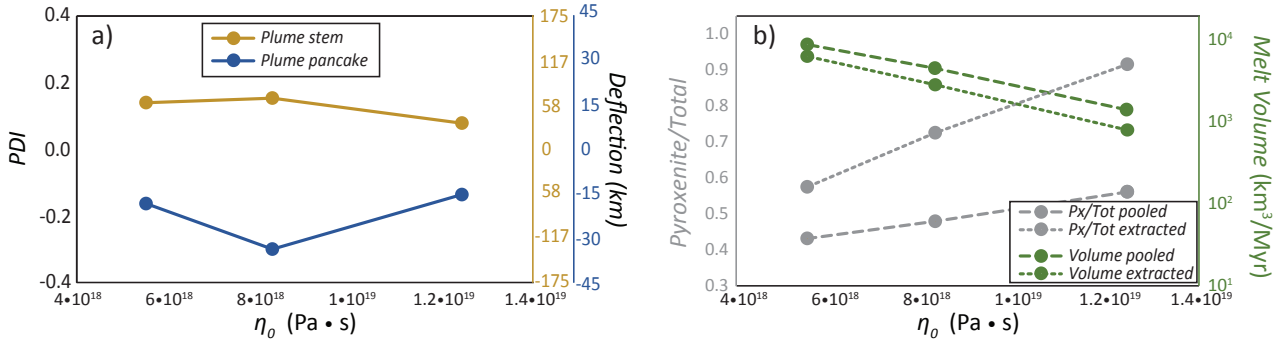

Figure 9. Diagrams showing the sensitivity of selected output parameters to η_0 in the steady state.

the low η_0 cases of the companion paper (Manjón-Cabeza Córdoba and Ballmer, 2021). We also find that the symmetry of the PET is higher for the cases with lower viscosity than for the case with intermediate and with high viscosity.

4 Discussion

We run a wide range of 3D numerical models to systematically explore the interaction between EDC and mantle plumes. One of our main results is that the plume geometry, its interaction with the lithosphere, and the extent of related melting depends on the distance of the plume from the edge, being altered by EDC. Despite these important effects, the buoyancy flux of the plume still remains the main influence on the characteristics of plume-lithosphere interaction and hotspot magmatism.

We quantify the deflection of plumes by two characteristic parameters: the deflection of the plume stem, and the deflection of the shallow plume conduit and the plume pancake. The plume stem is systematically deflected away from the edge. This may provide an explanation as to why hotspot tracks in the Atlantic preferentially occur near and sub-parallel to the continental margin, but rarely across it (an exception to this is the Cameroon Volcanic Line; Fitton, 1980; Déruelle et al., 2007). On the other hand, plume pancake deflection commonly (but not always) occurs towards the edge. This prediction may explain why some hotspot tracks (such as the Canaries) do not strictly align with plate velocity, and volcanism is widespread with more activity far from the continental margin than near to it (*e.g.*, La Palma vs. Gran Canaria).

The nature of the deflection of the plume pancake (and as well of the plume stem) systematically changes in our models with the distance of the plume to from the edge. However, this deflection is generally predicted to decrease with increasing B_{plume} (fig. 6a,c). Test cases with a greater step of lithospheric thickness at the continental margin confirm this prediction. Such a configuration implies greater downwelling fluxes of EDC (see Manjón-Cabeza Córdoba and Ballmer, 2021), and leads to greater deflections of the plume and more asymmetric plume-lithosphere interaction than the reference case. In terms of PDI, the absolute value of PDI_{stem} is 0.12, as opposed to 0.10 in the case with regular edge and similar parameters (fig. 7c);

https://doi.org/10.5194/egusphere-2022-15
Preprint. Discussion started: 23 March 2022

and PDI$_{pancake}$ is -0.07, as opposed to -0.05. A higher value for both indexes suggests that the plume-EDC interaction depends on the ratio between the downward flux of materials due to EDC and the upward flux of materials due to plume activity.

The dependence of plume-EDC interaction to these two fluxes agrees with previous work such as Ballmer et al. (2011), who found that, even for high plume fluxes, sublithospheric convective instabilities can have an effect on the surface expresion of mantle plumes. In turn, our results challenge the opinion that strong external fluxes will overprint or even ignore EDC (King and Anderson, 1998; Till et al., 2010; Kaislaniemi and Van Hunen, 2014), a statement that may need revision.

In contrast to the EDC-only cases in the first part of our work (Manjón-Cabeza Córdoba and Ballmer, 2021), volcanic (or melt) volume fluxes are significant, displaying strong variations as a function of plume parameters and moderate variations as a function of D_{plume}. Therefore, a subset of out models can account for the volumes of Eastern Atlantic hotspots. However, both B_{plume} and ΔT_{plume} also affect the geochemistry of the melts. Any increase in volcanism due to B_{plume} or ΔT_{plume} is associated with a decrease in enrichment ($i.e.$, the fraction of melting products from enriched lithologies such as pyroxenite. Figures. 4b, 6b,d), with only minor effects on geochemical proxies as a function of D_{plume} (fig. 8).

In the case of the Canary Islands, Carracedo et al. (1998) estimates a minimum volcanic flux of 4×10^2 km^3 Myr. In the companion paper (Manjón-Cabeza Córdoba and Ballmer, 2021), we clearly showed that EDC alone is insufficient to generate such magmatism, and that the contribution from a mantle plume (or equivalent source) is required. Our models predict that relatively weak plumes with parameters similar to that of the reference case are sufficient to generate these amounts of magmatism, but it remains difficult to pinpoint plume parameters, *e.g.*, as plume temperature and buoyancy flux trade off with each other (Figures 4b, 6b,d). This implies that the Canary plume must be of low flux ($i.e.$, B_{plume} < 200 kg s^{-1}), or low temperature ($i.e.$, ΔT_{plume} < 200 °C), but not both, as the melt volumes would be too low then ($i.e.$ < 10^2 km^3 Myr^{-1}). Note that M and V in the relevant model cases are of the same order of magnitude, suggesting that our results are robust despite model limitations and simplifications in terms of modeling mantle melting and extraction. Our predictions for $\frac{M_{PX}}{M}$ and $\frac{V_{PX}}{V}$ further constrain the properties of the plume: occurrence of shield-like magmas in the Canary Islands (Abdel-Monem et al., 1971, 1972; Carracedo et al., 1998) strengthen the suggestion that B_{plume} and ΔT_{plume} cannot (both) be lower than for our reference case, as this would generate too enriched melts.

The distance of the Canary hotspot from the African passive margin is ∼250-300 km. Considering the PDI values predicted for relatively weak plumes (figure 8b), we estimate that the Canary plume at 660 km depth is centered ∼50-100 km closer to the African margin than the hotspot (which is located near El Hierro). Likewise, we estimate that the plume is at 410 km depth is centered ∼30-70 km closer to the margin. This prediction is consistent with the receiver functions study of Saki et al. (2015): the location of the shallowest 410 km discontinuity is shifted from the hotspot at El Hierro eastward towards Lanzarote. In adition, the recent tomographic study of Civiero et al. (2021) shows an arcuate upper mantle plume beneath the Canaries not unlike the plumes shown in our study. Attending to this evidence, we estimate that the cases with 150≤ D_{plume} ≤250 km best match the configuration of the Canary plume. This finding implies that plume-EDC interaction (*e.g.*, as quantified by PDI values) is significant for the Canary hotspot. The plume stem is pushed to the west (away from the edge) by about 80-110 km and the plume pancake is pulled back to the east (towards the edge) about 25-35 km. If the volcanic flux at the Canaries

https://doi.org/10.5194/egusphere-2022-15
Preprint. Discussion started: 23 March 2022

is significantly higher than estimated by Carracedo et al. (1998), *e.g.* due to un-accounted magmatic crustal underplating, we reach the same conclusions, predicting very similar PDI values (figure 8c).

In addition, we find that several key characteristics of the Canary Islands are matched by our models. The Canaries present active volcanism far from the inferred deflection point of the plume stem near El Hierro (in fact, all islands are currently active with the exception of La Gomera; Abdel-Monem et al., 1971, 1972; Carracedo, 1999; Geldmacher et al., 2005). Several of our cases predict deflection of the plume pancake and the melting zones toward the continental margin (figure 5), including the cases with $150 \leq D_{plume} \leq 250$, which would explain the shape of the whole archipelago and the geographic distribution of volcanism. It is noteworthy that the PDI indexes of the figures above refer to thermal anomalies, and that the melting areas may be deflected even more than the thermal anomaly. Even with a plate velocity that would produce a volcanic track parallel to the ocean-continent transition, given the right distances to the edge, the plume pancake may not necessarily be parallel to the plate movement.

Another issue involves that the Canary hotspot may have moved in the last few million years westward with respect to the African margin (Wang et al., 2018). Accordingly, the distance of the hotspot relative to the African plate may have changed, which may render plume-EDC and plume-lithosphere interaction a transient phenomenon, which cannot be explicitly adressed by our steady-state model setting. However, figures 7 and 8 provide an indication of how the geometry of the plume and plume-lithosphere interaction may have changed during such a movement. As the plume moves away from the margin, the effects of changes in plume-EDC interaction may have extended and deflected the pancake and, therefore, extended the area of volcanism from a single track to a wide zone (Geldmacher et al., 2005). Our model predicts that, eventually, further movement of the plume away from the edge may decrease the extent of plume deflection. Alternatively, if the vigor of the plume (or of EDC) has recently changed, plume-EDC interaction and plume displacement would have also changed, and the movement of the hotspot relative to the African margin would be potentially unrelated to any movement of the deep plume stem or even the plate movement.

The application of our models to other hotspots in the Eastern Atlantic is less obvious. Lodhia et al. (2018) and King and Ritsema (2000) have suggested a link between the Cape Verde plume and the downwelling at the African Margin near Cape Verde. From our models, however, a significant effect of EDC on plume ascent over such long distances (over 1000 km) is not justified. It is true that higher mantle viscosities may result in larger EDC cells, but it will also result in lower EDC-related fluxes as already shown in figure 5a of Manjón-Cabeza Córdoba and Ballmer (2021). Regardless, the models presented here include a plate velocity that is not fully consistent with the Cape Verde 'near-zero' plate velocity. In fact, Patriat and Labails (2006) detected a "bulge" or "bum" along the continental-oceanic transition between the Canary Islands and Cape Verde. Whether this "bulge" is related to an EDC upwelling is difficult to determine, but a topography high is expected in the area of maximum sub-lithospheric erosion above an EDC upwelling (Manjón-Cabeza Córdoba and Ballmer, 2021). Such a relationship is also consistent with lithospheric models that detect EDC-related erosion at the bottom of the lithosphere beneath the Canaries (see for instance figure 7, model c2 of Fullea et al., 2015), which would imply that the main EDC upwelling happens very close to the edge. Such a proximity is also suggested by our 3D models here. The aforementioned "bulge" is consistent with the location of the eastern islands of the Canary archipelago, but does not seem to be related directly to the Cape Verde hotspot.

https://doi.org/10.5194/egusphere-2022-15
Preprint. Discussion started: 23 March 2022

To fully solve the Canary puzzle and test the hypotheses proposed here, further work is required. One of the main characteristics of the Canary Islands hotspot is the near absence of a hotspot swell. Analysis of dynamic topography using geodynamic models may answer whether deflection of the plume and the pancake by EDC can blur the dynamic-topography signal of the plume (Huppert et al., 2020). Another area of potential further work is to better constrain the geochemical fingerprint of our model magmas. In our models, ΔT_{plume} and B_{plume} have very similar effects on the compositional proxies of volcanism used here ($\frac{M_{PX}}{M}$ and $\frac{V_{PX}}{V}$). However, as soon as several geochemical systems are considered (*e.g.*, major and trace elements, isotopes), the effects of ΔT_{plume} should have a distinct effect on the geochemistry of magmas from increasing B_{plume}. Unfortunately, additional assumptions in terms of starting composition of PX and peridotite are required to explicitly predict trace-element and isotopic signatures (Bianco et al., 2008). Moreover, no practical melting parameterization is available to realistically predict major element compositions from geodynamic models. Future work will focus on a new melting parameterization that can help to discriminate between parameters in this setting and other geodynamic models.

5 Conclusions

We studied the effects of Edge-Driven Convection (EDC) on low-to-intermediate buoyancy flux plumes. The following points summarize the main findings of this study:

- Low and intermediate buoyancy flux plumes interact with shallow mantle flow related to sub-lithospheric convective instability, which cause the plume to be deflected with important effects on the volume flux (and composition) of hotspot melting.
- The interaction of the plume with Edge-Driven Convection highly depends on the distance of the plume to the ocean-continent transition, but the distance for which EDC has the strongest influence varies with physical properties of the mantle and plumes. For example, weaker plumes (lower buoyancy flux, lower temperature) are most affected closer to the edge (*i.e.*, continental margin) than more vigorous plues plumes (higher buoyacy flux, higher temperature).
- The ratio of the buoyancy flux of the plume with respect to the flux of material from EDC is one of the most important factors to control plume-EDC interaction at a given plume-edge distance, including deflection of the plume stem away from the continental edge, and of the pancake towards the Edge.
- In the Canary Islands, a plume of low buoyancy flux and high temperature or, alternatively, a plume with moderate buoyancy flux and low temperature may be rising at 200 km from the continental margin, being deflected and creating the complex age progression and widespread volcanism.

Code availability. CITCOM CU (Moresi and Solomatov, 1995; Moresi and Gurnis, 1996; Zhong et al., 2000) is an open source code available at https://geodynamics.org/cig/software/citcomcu/. The modified version of CITCOM CU with the modifications described in the text is available at https://doi.org/10.5281/zenodo.4293656

https://doi.org/10.5194/egusphere-2022-15
Preprint. Discussion started: 23 March 2022

Author contributions. AMCC performed the numerical experiments and post-processed, analyzed and plotted the data. Both authors devised the study, interpreted results and wrote the paper.

Competing interests. We decleare that we do not have any competing interest.

Acknowledgements. AMCC was funded by the Schweizerischer Nationalfonds zur Förderung der Wissenschaftlichen Forschung (grant no. 2-77026-16).

https://doi.org/10.5194/egusphere-2022-15
Preprint. Discussion started: 23 March 2022

References

Abdel-Monem, A., Watkins, N. D., and Gast, P. W.: Potassium-Argon Ages, Volcanic Stratigraphy, and Geomagnetic Polarity History of the Canary Islands: Lanzatorte, Fuerteventura, Gran Canaria y La Gomera, American Journal of Science, 271, 490–521, http://www.ajsonline.org/content/271/5/490.full.pdf, 1971.

Abdel-Monem, A., Watkins, N. D., and Gast, P. W.: Potassium-Argon Ages, Volcanic Stratigraphy and Geomagnetic Polarity History of the Canary Islands: Tenerife, La Palma, and Hierro, American Journal of Science, 272, 805–825, http://www.ajsonline.org/content/272/9/805.full.pdf, 1972.

Ballmer, M. D., van Hunen, J., Ito, G., Tackley, P. J., and Bianco, T. A.: Non-hotspot volcano chains originating from small-scale sublithospheric convection, Geophysical Research Letters, 34, https://doi.org/10.1029/2007GL031636, 2007.

Ballmer, M. D., van Hunen, J., Ito, G., Bianco, T. A., and Tackley, P. J.: Intraplate volcanism with complex age-distance patterns: A case for small-scale sublithospheric convection, Geochemistry, Geophysics, Geosystems, 10, https://doi.org/10.1029/2009GC002386, 2009.

Ballmer, M. D., Ito, G., Van Hunen, J., and Tackley, P. J.: Spatial and temporal variability in Hawaiian hotspot volcanism induced by small-scale convection, Nature Geoscience, 4, 457–460, https://doi.org/10.1038/ngeo1187, 2011.

Bianco, T. A., Ito, G., van Hunen, J., Ballmer, M. D., and Mahoney, J. J.: Geochemical variation at the Hawaiian hot spot caused by upper mantle dynamics and melting of a heterogeneous plume, Geochemistry, Geophysics, Geosystems, 9, Q11 003, https://doi.org/10.1029/2008GC002111, 2008.

Carracedo, J. C.: Growth, structure, instability and collapse of Canarian volcanoes and comparisons with Hawaiian volcanoes, Journal of Volcanology and Geothermal Research, 94, 1–19, https://doi.org/10.1016/S0377-0273(99)00095-5, 1999.

Carracedo, J. C., Day, S., Guillou, H., Rodríguez Badiola, E., Canas, J. A., and Pérez Torrado, F. J.: Hotspot volcanism close to a passive continental margin: the Canary Islands, Geological Magazine, 135, 591–604, https://www.cambridge.org/core/journals/geological-magazine/article/hotspot-volcanism-close-to-a-passive-continental-margin-the-canary-islands/26D6FD3C9CA2DAC201366C987DBAFC31, 1998.

Civiero, C., Custódio, S., Neres, M., Schlaphorst, D., Mata, J., and Silveira, G.: The Role of the Seismically Slow Central-East Atlantic Anomaly in the Genesis of the Canary and Madeira Volcanic Provinces, Geophysical Research Letters, 48, 1–15, https://doi.org/10.1029/2021GL092874, 2021.

Conrad, C. P., Wu, B., Smith, E. I., Bianco, T. A., and Tibbetts, A.: Shear-driven upwelling induced by lateral viscosity variations and asthenospheric shear: A mechanism for intraplate volcanism, Physics of the Earth and Planetary Interiors, 178, 162–175, https://doi.org/10.1016/J.PEPI.2009.10.001, 2010.

Courtillot, V., Davaille, A., Besse, J., and Stock, J.: Three distinct types of hotspots in the Earth's mantle, Earth and Planetary Science Letters, 205, 295–308, https://doi.org/10.1016/S0012-821X(02)01048-8, 2003.

Déruelle, B., Ngounouno, I., and Demaiffe, D.: The 'Cameroon Hot Line' (CHL): A unique example of active alkaline intraplate structure in both oceanic and continental lithospheres, Comptes Rendus - Geoscience, 339, 589–600, https://doi.org/10.1016/j.crte.2007.07.007, 2007.

Doblas, M., Lo´pez-Ruiz, J., and Cebria´, J.-M.: Cenozoic evolution of the Alboran Domain: A review of the tectonomagmatic models, in: Cenozoic Volcanism in the Mediterranean Area, vol. 418, pp. 303–320, Geological Society of America, https://doi.org/10.1130/2007.2418(15), 2007.

https://doi.org/10.5194/egusphere-2022-15
Preprint. Discussion started: 23 March 2022

Duggen, S., Hoernle, K. A., Hauff, F., Klügel, A., Bouabdellah, M., and Thirlwall, M. F.: Flow of Canary mantle plume material through a subcontinental lithospheric corridor beneath Africa to the Mediterranean, Geology, 37, 283–286, https://doi.org/10.1130/G25426A.1, 2009.

Dumoulin, C., Doin, M. P., Arcay, D., and Fleitout, L.: Onset of small-scale instabilities at the base of the lithosphere: Scaling laws and role of pre-existing lithospheric structures, Geophysical Journal International, 160, 345–357, https://doi.org/10.1111/j.1365-246X.2004.02475.x, 2005.

Duvernay, T., Davies, D. R., Mathews, C. R., Gibson, A. H., and Kramer, S. C.: Linking Intra-Plate Volcanism to Lithospheric Structure and Asthenospheric Flow, Geochemistry, Geophysics, Geosystems, i, e2021GC009 953, https://doi.org/10.1029/2021GC009953, 2021.

Fitton, J. G.: The Benue Trough and Cameroon Line - A migrating rift system in West Africa, Earth and Planetary Science Letters, 51, 132–138, 1980.

French, S. W. and Romanowicz, B.: Broad plumes rooted at the base of the Earth's mantle beneath major hotspots, Nature, 525, 95–99, https://doi.org/10.1038/nature14876, 2015.

Fullea, J., Camacho, A. G., Negredo, A. M., and Fernández, J.: The Canary Islands hot spot: New insights from 3D coupled geophysical-petrological modelling of the lithosphere and uppermost mantle, Earth and Planetary Science Letters, https://doi.org/10.1016/j.epsl.2014.10.038, 2015.

Geldmacher, J., Hoernle, K., Bogaard, P. V., Duggen, S., and Werner, R.: New ^{40}/Ar^{39}Ar age and geochemical data from seamounts in the Canary and Madeira volcanic provinces: Support for the mantle plume hypothesis, Earth and Planetary Science Letters, 237, 85–101, https://doi.org/10.1016/j.epsl.2005.04.037, 2005.

Helffrich, G., Faria, B., Fonseca, J. F., Lodge, A., and Kaneshima, S.: Transition zone structure under a stationary hot spot: Cape Verde, Earth and Planetary Science Letters, 289, 156–161, https://doi.org/10.1016/j.epsl.2009.11.001, 2010.

Hirschmann, M. M. and Stolper, E. M.: A possible role for garnet pyroxenite in the origin of the "garnet signature" in MORB, Contributions to Mineralogy and Petrology, 124, 185–208, https://doi.org/10.1007/s004100050184, 1996.

Huang, J., Zhong, S. J., and van Hunen, J.: Controls on sublithospheric small-scale convection, Journal of Geophysical Research, 108, https://doi.org/10.1029/2003JB002456, 2003.

Huppert, K. L., Perron, J. T., and Royden, L. H.: Hotspot swells and the lifespan of volcanic ocean islands, Science Advances, 6, eaaw6906, https://doi.org/10.1126/sciadv.aaw6906, 2020.

Kaislaniemi, L. and Van Hunen, J.: Dynamics of lithospheric thinning and mantle melting by edge-driven convection: Application to Moroccan Atlas mountains, Geochemistry, Geophysics, Geosystems, 15, 3175–3189, https://doi.org/10.1002/2014GC005414, 2014.

Kim, D.-H. and So, B.-D.: Effects of rheology and mantle temperature structure on edge-driven convection: Implications for partial melting and dynamic topography, Physics of the Earth and Planetary Interiors, 303, 106 487, https://doi.org/10.1016/j.pepi.2020.106487, 2020.

King, S. D. and Adam, C.: Hotspot swells revisited, Physics of the Earth and Planetary Interiors, 235, 66–83, https://doi.org/10.1016/j.pepi.2014.07.006, 2014.

King, S. D. and Anderson, D. L.: An alternative mechanism of flood basalt formation, Earth and Planetary Science Letters, 136, 269–279, https://doi.org/10.1016/0012-821X(95)00205-Q, 1995.

King, S. D. and Anderson, D. L.: Edge-driven convection, Earth and Planetary Science Letters, 160, 289–296, https://doi.org/10.1016/S0012-821X(98)00089-2, 1998.

King, S. D. and Ritsema, J.: African Hot Spot Volcanism: Small-Scale Convection in the Upper Mantle Beneath Cratons, Science, 290, 1137–1139, http://science.sciencemag.org/, 2000.

https://doi.org/10.5194/egusphere-2022-15
Preprint. Discussion started: 23 March 2022

Korenaga, J. and Jordan, T. H.: Linear stability analysis of Richter rolls, Geophysical Research Letters, 30, https://doi.org/10.1029/2003GL018337, 2003.

Liu, X. and Zhao, D.: Seismic evidence for a mantle plume beneath the Cape Verde hotspot, International Geology Review, 56, 1213–1225, https://doi.org/10.1080/00206814.2014.930720, 2014.

Lodhia, B. H., Roberts, G. G., Fraser, A. J., Fishwick, S., Goes, S., and Jarvis, J.: Continental margin subsidence from shallow mantle convection: Example from West Africa, Earth and Planetary Science Letters, 481, 350–361, https://doi.org/10.1016/j.epsl.2017.10.024, 2018.

Manjón-Cabeza Córdoba, A. and Ballmer, M. D.: The role of edge-driven convection in the generation of volcanism - Part 1: A 2D systematic study, Solid Earth, 12, 613–632, https://doi.org/10.5194/se-12-613-2021, 2021.

Marquart, G.: On the geometry of mantle flow beneath drifting lithospheric plates, Geophysical Journal International, 144, 356–372, https://doi.org/10.1046/j.0956-540X.2000.01325.x, 2001.

Martín, A., Sevilla, M., and Zurutuza, J.: Crustal deformation study in the Canary Archipelago by the analysis of GPS observations, Journal of Applied Geodesy, 8, 129–140, https://doi.org/10.1515/jag-2014-0002, 2014.

Martínez-Arevalo, C., Mancilla, F. d. L., Helffrich, G., and García, A.: Seismic evidence of a regional sublithospheric low velocity layer beneath the Canary Islands, Tectonophysics, 608, 586–599, https://doi.org/10.1016/j.tecto.2013.08.021, 2013.

Milelli, L., Fourel, L., and Jaupart, C.: A lithospheric instability origin for the Cameroon Volcanic Line, Earth and Planetary Science Letters, 335-336, 80–87, https://doi.org/10.1016/j.epsl.2012.04.028, 2012.

Moresi, L. N. and Gurnis, M.: Constraints on the lateral strength of slabs from three-dimensional dynamic flow models, Earth and Planetary Science Letters, 138, 15–28, https://doi.org/10.1016/0012-821x(95)00221-w, 1996.

Moresi, L. N. and Solomatov, V. S.: Numerical investigation of 2D convection with extremely large viscosity variations, Physics of Fluids, 7, 2154–2162, https://doi.org/10.1063/1.868465, 1995.

Morgan, W. J.: Convection Plumes in the Lower Mantle, Nature, 230, 42–43, https://doi.org/10.1038/230042a0, 1971.

Müller, R. D., Sdrolias, M., Gaina, C., and Roest, W. R.: Age, spreading rates, and spreading asymmetry of the world's ocean crust, Geochemistry, Geophysics, Geosystems, 9, Q04 006, https://doi.org/10.1029/2007GC001743, 2008.

Parsons, B. and McKenzie, D.: Mantle convection and the thermal structure of the plates, Journal of Geophysical Research, 83, 4485–4496, https://doi.org/10.1029/jb083ib09p04485, 1978.

Patriat, M. and Labails, C.: Linking the Canary and Cape-Verde Hot-Spots, Northwest Africa, Marine Geophysical Researches, 27, 201–215, https://doi.org/10.1007/s11001-006-9000-7, 2006.

Ribe, N. M. and Christensen, U. R.: Three-dimensional modeling of plume-lithosphere interaction, Journal of Geophysical Research, 99, 669–682, https://doi.org/10.1029/93JB02386, 1994.

Richter, F. M.: Convection and the large-scale circulation of the mantle, Journal of Geophysical Research, 78, 8735–8745, https://doi.org/10.1029/jb078i035p08735, 1973.

Richter, F. M. and Parsons, B.: On the interaction of two scales of convection in the mantle, Journal of Geophysical Research, 80, 2529–2541, https://doi.org/10.1029/jb080i017p02529, 1975.

Saki, M., Thomas, C., Nippress, S. E., and Lessing, S.: Topography of upper mantle seismic discontinuities beneath the North Atlantic: The Azores, Canary and Cape Verde plumes, Earth and Planetary Science Letters, 409, 193–202, https://doi.org/10.1016/J.EPSL.2014.10.052, 2015.

https://doi.org/10.5194/egusphere-2022-15
Preprint. Discussion started: 23 March 2022

Schellart, W., Stegman, D., and Freeman, J.: Global trench migration velocities and slab migration induced upper mantle volume fluxes: Constraints to find an Earth reference frame based on minimizing viscous dissipation, Earth-Science Reviews, 88, 118–144, https://doi.org/10.1016/j.earscirev.2008.01.005, 2008.

Sleep, N. H.: Hotspots and mantle plumes: Some phenomenology, Journal of Geophysical Research, 95, 6715–6736, https://doi.org/10.1029/JB095iB05p06715, 1990.

Thirlwall, M. F., Singer, B. S., and Marriner, G. F.: ^{39}Ar ^{40}Ar ages and geochemistry of the basaltic shield stage of Tenerife, Canary Islands, Spain, Journal of Volcanology and Geothermal Research, 103, 247–297, www.elsevier.nl/locate/jvolgeores, 2000.

Till, C. B., Elkins-Tanton, L. T., and Fischer, K. M.: A mechanism for low-extent melts at the lithosphere-asthenosphere boundary, Geochemistry, Geophysics, Geosystems, https://doi.org/10.1029/2010GC003234, 2010.

Wang, S., Yu, H., Zhang, Q., and Zhao, Y.: Absolute plate motions relative to deep mantle plumes, Earth and Planetary Science Letters, 490, 88–99, https://doi.org/10.1016/j.epsl.2018.03.021, 2018.

Wilson, J. T.: A Possible Origin of the Hawaiian Islands, Canadian Journal of Physics, 41, 863–870, https://doi.org/10.1139/p63-094, 1963.

Zhong, S. J., Zuber, M. T., Moresi, L. N., and Gurnis, M.: Role of temperature-dependent viscosity and surface plates in spherical shell models of mantle convection, Journal of Geophysical Research: Solid Earth, 105, 11 063–11 082, https://doi.org/10.1029/2000JB900003, 2000.